

# Structural, Morphological, Optical and Electrical Properties of $Y^{3+}$ Doped $Ni_{1-x}Cd_xFe_{2-y}O_4$ Spinel Nanoferrite

R. B. Bhise<sup>1,2</sup>, S. M. Rathod<sup>3</sup>

<sup>1</sup>Department of Physics, B. J. College, Ale, Tal: Junnar, Dist: Pune, 412411, India

<sup>2</sup>Science College, SRTM University, Nanded, India

<sup>3</sup>Nanomaterials and Laser Research Laboratory, Abasaheb Garware College, Pune, 411004, India

**Abstract:** Structural, morphological, optical and electrical properties are investigated  $Y^{3+}$  doped  $Ni_{1-x}Cd_xFe_{2-y}O_4$  spinel nanoferrite (where  $x = 0, 0.2, 0.4, 0.6$  and  $y = 0$  and  $0.075$ ) were obtained by sol-gel autocombustion techniques. Nanophase samples were carried out at low temperature and cost effective method with analytical grade metal nitrate. Citric acid was used as a fuel. The prepared powder were sintered at  $400^\circ C$  and characterized by X-ray diffraction (XRD), Energy dispersive X-ray spectroscopy (EDAX) for structural property, scanning electron microscopy (SEM), Transmission electron microscopy (TEM) for morphological studies and absorption spectra studied using infrared (FTIR) characterization. Ferrite formation was found to quite sensitive. The particle size was determined using Scherer's formula and it found that it decreases with increase in  $Y^{3+}$  content. Also DC resistivity increases with increasing  $Y^{3+}$  content and electrical conductivity increases with temperature increases. These results may be applicable for promising area such as high frequency electrical devices.

**Keywords:** Spinel Ferrite; Sol-gel autocombustion method; Morphological properties; Optical properties; Electrical properties;

## 1. Introduction

The spinel structure of nanoferrites possesses the general formula of  $[A][B_2]O_4$ , where A refers to cations in tetrahedral sites (where,  $A = Co^{2+}, Ni^{2+}, Mn^{2+}, Mg^{2+}, Zn^{2+}, Cd^{2+}$ ) which is a class of hybrid functional materials and B represents the cations in the octahedral positions in a cubic structure. The formula  $[A_{1-x}B_x][A_yB_{2-y}]O_4$  represents many possible intermediary distributions that denote considerable cations disorder, indicating that this structure requires special attention in terms of magnetic characterization [1]. The physical properties such as increase in DC resistivity, low dielectric losses and magnetization characteristics are due to the substitution of tetrahedral cations in the parent crystal structure. The structural variation in the host lattice can be occurred due to proper choice and composition of trivalent cations such as  $Al^{3+}, Y^{3+}, Cr^{3+}$  and  $La^{3+}$ ) to replace  $Fe^{3+}$  in the parent lattice of cobalt ferrite [2]. Electrical and magnetic properties of ferrites mainly depend on their chemical composition, preparation method, sintering time and temperature, distribution of the cations in tetrahedral and octahedral sites and range of deficiency in the chemical composition [3]. The sol-gel method is used for the synthesis of Nickel substituted cobalt ferrite nanoparticles. The result proves that with increase in nickel content magnetic saturation decreases [4]. The sol-gel method is a good combination of combustion and chemical gel process. The advantage of sol-gel method is a good stoichiometric control and results in ultra-fine nano particles [5]. Infrared spectroscopy (IR) is one of the most powerful techniques, which offers possibility of chemical identification. One of the advantages of IR over other methods for structural analysis is that, it provides useful information about the structure of a molecule rapidly and also without cumbersome evaluation methods. The technique is based upon the simple fact that a chemical substance shows

marked selective adsorption in the infrared region. Various bands obtained in IR spectra are corresponding to the characteristic functional groups and bonds present in the chemical substance. The absorption bands in the IR spectra split on the basis of different cations present on tetrahedral (A) and octahedral [B] sites of spinel ferrites [6-8]. Nickel ferrites are stable, relatively inexpensive and easily manufactured and have wide applications in electronics and communication industries owing to their interesting magnetic and electrical properties. The coercivity was decreased by increasing Cd content due to the decrease of magneto crystalline anisotropy constant of the samples [9]. Yttrium doped cobalt ferrite was prepared with different concentrations to identify the crystallite size with respect to the yttrium concentration, temperature and changes in the structural and electrical properties and reported that the resistance of the nano structured yttrium doped cobalt ferrites nano powders was analyzed. The resistance was increased by the addition of yttrium to cobalt ferrites [10].

The present work investigation on the synthesis of nano-sized  $Y^{3+}$  material substituted in Ni-Cd nanocrystalline ferrites by sol-gel autocombustion techniques and characterized by XRD, EDAX, FTIR, SEM and TEM. It reports the consequent changes on their structural, optical, morphological and electrical properties. Yttrium doped Ni-Cd nanoferrites were synthesized with average grain size ranging between 12.5 to 34.8 nm which will give great effect on it electric properties.

## 2. Material and Method

The  $Y^{3+}$  doped in Ni-Cd ferrite powders were synthesized by sol-gel auto combustion method at low temperatures for different compositions of  $Ni_{1-x}Cd_xY_yFe_{2-y}O_4$  (Where  $x = 0.0, 0.2, 0.4, 0.6$ , and  $y = 0.0$  and  $0.075$ ). The AR grade

nitrate of Merck company (purity of 99%) are used in the experiments such as Yttrium nitrate ( $Y(NO_3)_3 \cdot 6H_2O$ ), Nickel nitrate ( $Ni(NO_3)_2 \cdot 6H_2O$ ), Cadmium nitrate ( $Cd(NO_3)_2 \cdot 6H_2O$ ), Ferric nitrate ( $Fe(NO_3)_3 \cdot 9H_2O$ ). These nitrates and citric acid are using stoichiometric ratio proportion to obtain the final product and the citric acid ( $C_6H_8O_7$ ) is used as a fuel in the ratio 1:3. The proportion of each reagent was defined according to its respective molar amounts [11]. All chemicals are dissolved in distilled water and were stirred till to obtain the homogeneous solution. To maintain pH equal to 7 by adding drop by drop ammonium hydroxide ( $NH_4OH$ ) during the stirring process. This solution was stirred continuously with  $80^\circ C$  for about 4-5 hours to obtain sol. After 4-5 hours, gel converts into ash and ash convert into powder. Finally get fine powder of  $Ni_{1-x}Cd_xY_yFe_{2-y}O_4$  ferrite nanoparticles after auto combustion. The powder was sintered at  $400^\circ C$  for 2 hours.

Various analytical tools like X-ray diffraction (XRD), Energy dispersive x-ray spectroscopy (EDAX), Fourier transformation infrared (FTIR), Scanning electron microscopy (SEM), and Transmission electron microscopy (TEM) were used for the characterization and evaluation of properties. The structural characterization was done using XRD analysis. The X-ray diffractometer with Cu-K $\alpha$  radiation of wavelength  $1.5405 \text{ \AA}$  at 40 kV performed a scanning from 20 to 80 degree at a step size of 0.02 degree per second for each prepared sample and determined crystal structure, lattice parameter and crystallite size. The microstructure investigations were carried out on the fracture surfaces of the samples using thermal field emission scanning electron microscope (SEM, JSM-7600F) equipped with an energy dispersive x-ray spectroscopy (EDAX). The optical characteristics was studied using Fourier Transformation Infrared (FT-IR) of Bruker 3000 Hyperion microscope with vertex 80 single point detector performing images resolution ranging between 7500 to  $450 \text{ cm}^{-1}$ . The particle morphology was studied using Scanning electron microscopy (SEM) of JEOL JSM-7600F combines two proven technologies operating at 0.1 to 30 kV with high resolution and Transmission electron microscopy (TEM) of PHILIPS CM-200 operating at 20-200 kV with resolution  $2.4 \text{ \AA}$ . The temperature dependence of DC resistivity of samples was recorded at different temperature  $200^\circ C$  and  $300^\circ C$  with USB computer interface through SES-CAMM module using electrometer (TPX-600C having resolution 1

pA to 100 nA) in two probe method. Further investigations of the electrical properties are under way to elucidate the effective role of inter particle interactions in these samples.

### 3. Results and Discussion

#### 3.1 Structural Studies

**a) XRD analysis:** The resulting powder  $Ni_{1-x}Cd_xY_yFe_{2-y}O_4$  (where  $x = 0, 0.2, 0.4, 0.6$  and  $y = 0$  and  $0.075$ ) nano crystals were characterized by XRD pattern. The XRD pattern of sintered  $Y^{3+}$  doped the nickel-cadmium ferrite nano crystals as shown in figure-1(a). Obtained XRD pattern and crystalline phases were identified and it conforms the formation of a homogeneous well-defined spinal cubic structure with put any impurity. The broad peaks in the XRD pattern indicate a fine particle nature of the particles. The particle size was determined using Scherer's formula,

$$t = \frac{0.9 \lambda}{\beta \cos \theta}$$

Where,  $\lambda$  = wavelength of X-ray used,  $\theta$  = peak position and  $\beta$  = FWHM of the peak  $\theta$  and it is corrected for instrumental broadening. The average particle sizes of nanoparticles are given in Table-1. The particle size decreases as the concentration of  $Y^{3+}$  increases. Lattice parameter obtained for prepared sample is ranging between  $8.3399$  to  $8.3665 \text{ \AA}$ . The deviation in lattice parameter can be attributed to the cations rearrangement in the nano sized prepared ferrites. Value of lattice constant for Cd and Ni doped Yttrium ferrite shows the expansion of unit cell with rare earth doping when compared with pure Yttrium ferrite. This is expected due to substitution of large ionic radius of  $Y^{3+}$  ions ( $0.9 \text{ \AA}$ ) with small ionic radius  $Fe^{3+}$  ions ( $0.645 \text{ \AA}$ ). This result in  $Y^{3+}$  substituted ferrites to have higher thermal stability relative to Ni-Cd ferrite.

**Table 1:** The particle size of  $Ni_{1-x}Cd_xY_yFe_{2-y}O_4$  by XRD

Obs. No.	Composition	Average grain size (t) nm	Lattice constant (a) $\text{\AA}$
1	$NiFe_2O_4$	34.7791	8.3399
2	$Ni_{0.8}Cd_{0.2}Fe_2O_4$	25.158	8.3455
3	$Ni_{0.8}Cd_{0.2}Y_{0.075}Fe_{1.925}O_4$	20.762	8.3591
4	$Ni_{0.6}Cd_{0.4}Y_{0.075}Fe_{1.925}O_4$	16.052	8.3635
5	$Ni_{0.4}Cd_{0.6}Y_{0.075}Fe_{1.925}O_4$	12.498	8.3665

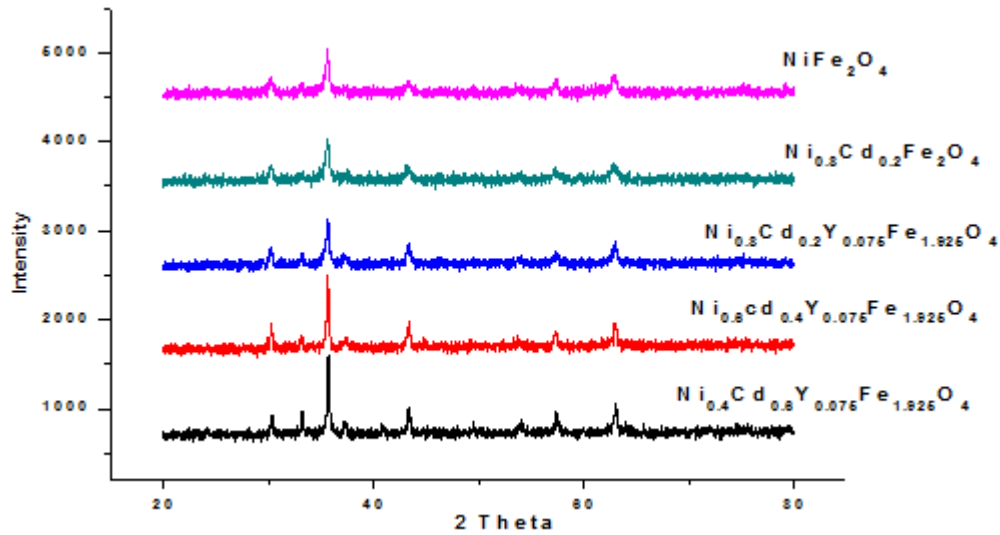


Figure 1 (a): Structural properties of  $Ni_{1-x}Cd_xY_yFe_{2-y}O_4$  by XRD

**b) EDAX analysis:** The typical EDAX spectra taken from the ferrite grain and grain boundary of a typical sample  $Ni_{0.4}Cd_{0.6}Y_{0.075}Fe_{1.925}O_4$  to know the chemical constituents present in the materials and it reveals that the ferrite grain contain amount of  $Y^{3+}$  supporting indirectly the entering of yttrium ions into the sub lattice of ferrites. The EDAX spectra shows the content of  $Y^{3+}$  is less than that of its

normal composition due to segregation of yttrium ions into the grain boundaries and evaporation at high temperature. Also it is found that grain sizes of the samples decreases with increasing in doping of  $Y^{3+}$  ions because more cations vacancies, closed pores exist and grain boundary movement when large amount of  $Y^{3+}$  ions exist in the samples.

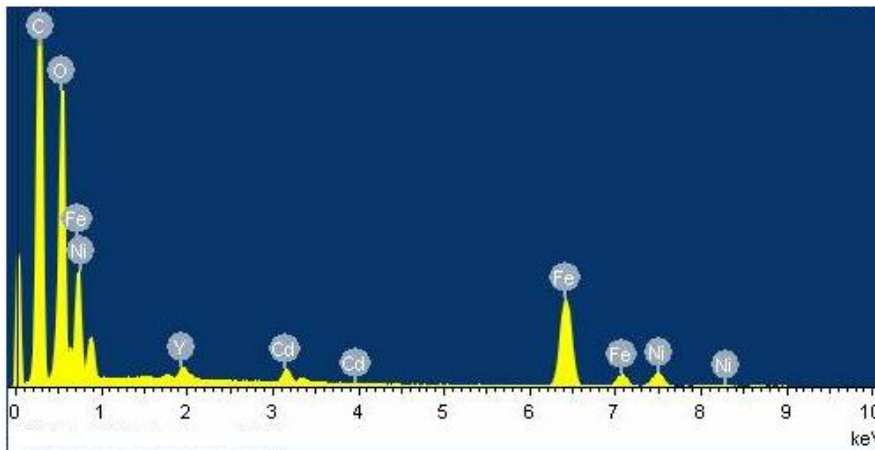
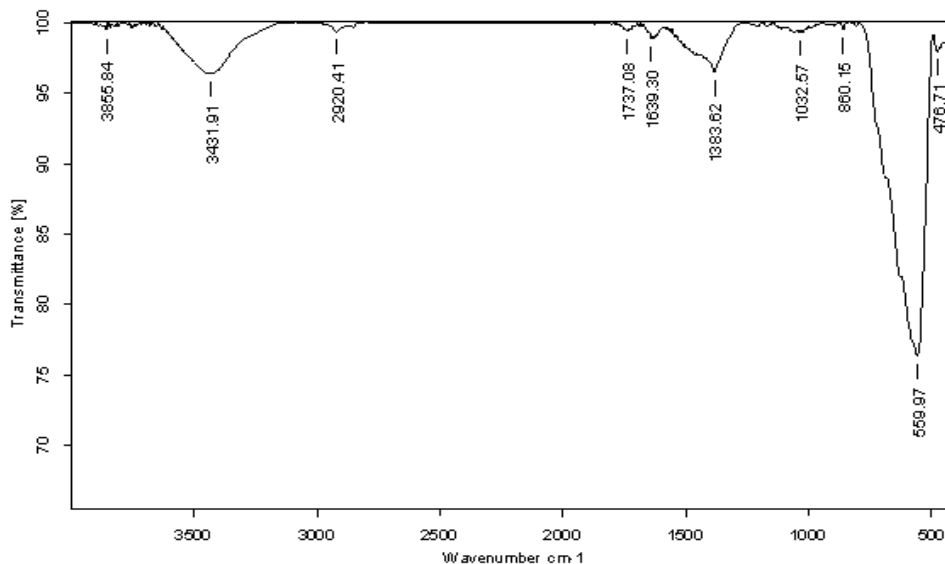


Figure 1(b): Structural properties of  $Ni_{0.4}Cd_{0.6}Y_{0.075}Fe_{1.925}O_4$  by EDAX

### 3.2 Optical studies



**Figure 2:** Absorption spectra of  $\text{Ni}_{0.6}\text{Cd}_{0.4}\text{Y}_{0.075}\text{Fe}_{1.925}\text{O}_4$  by FT-IR

The FTIR spectra of the prepared  $\text{Ni}_{0.6}\text{Cd}_{0.4}\text{Y}_{0.075}\text{Fe}_{1.925}\text{O}_4$  are shown in figure 2 to know the bonding characteristics of the materials. The peaks at  $476.71\text{ cm}^{-1}$  and  $559.97\text{ cm}^{-1}$  are the peaks of Fe-O bond in Y-Ni-Cd ferrite and it arises due to the lattice vibrations of the oxide ions against cations. The peak at  $1383.62\text{ cm}^{-1}$  indicates the presence of O-H bond due to bending vibration. The broad peak at  $3431.91\text{ cm}^{-1}$  gives presence of hydroxyl group in the material and indicates that the material absorbed moisture from atmosphere during analysis. The intense absorption bond is observed at  $559.97\text{ cm}^{-1}$  which shows the characteristic bond of spinel structure which may due to presence of Fe-O and Y-O bonds or crystalline nature of Y doped Ni-Cd ferrite. Hence, FTIR analysis supports the observation of XRD analysis and confirmed the crystalline nature of ferrite. So, the peaks at  $416\text{ cm}^{-1}$  and  $860\text{ cm}^{-1}$  have confirmed the presence of Ni-Cd ferrite and the peaks at  $476\text{ cm}^{-1}$  and  $1032\text{ cm}^{-1}$  have confirms the presence of yttrium. Finally the doping of  $\text{Y}^{3+}$  on Ni-Cd ferrite was confirmed by different

pattern of the plots and the difference in relative position and intensity of the peaks appeared in the FTIR plots of the prepared samples.

### 3.3 Morphological Studies

**a) SEM analysis:** The SEM images of Ni-Cd nanocrystalline ferrites by sol-gel auto combustion method as shown in figure-3. The SEM image of the prepared  $\text{Ni}_{0.8}\text{Cd}_{0.2}\text{Y}_{0.075}\text{Fe}_{1.92}\text{O}_4$  samples is composed of nano crystals and shows the distribution of nanoparticles. The calculated ferrite grain sizes of the corresponding Yttrium doped Ni-Cd ferrite samples from these graphs are presented in table 1. It is observed that the grain sizes of the ferrites in the samples decreases with increase in doping of  $\text{Y}^{3+}$  ions that indicates increase in grain size is not liquid-phase sintering. The melting point of  $\text{Y}^{3+}$  is  $1522\text{ }^{\circ}\text{C}$  which is much larger than the sintering temperature ( $400\text{ }^{\circ}\text{C}$ ) of the ferrites.

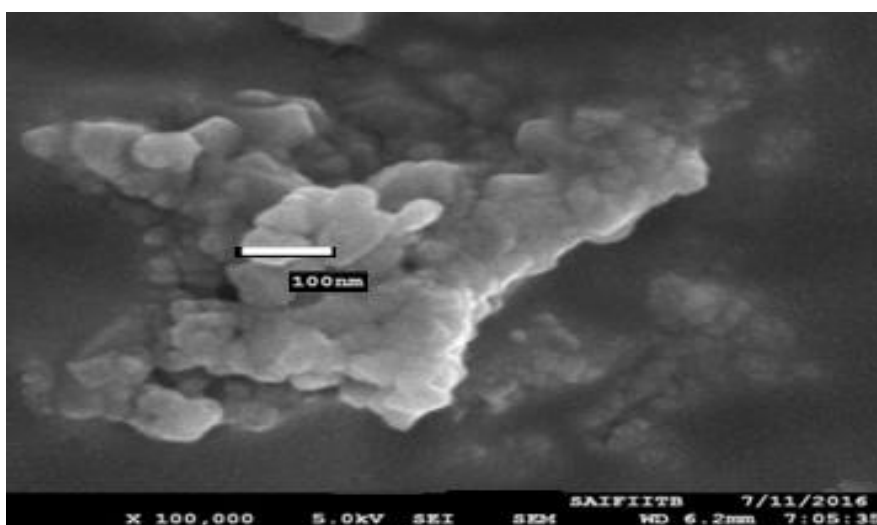


**Figure 3:** Morphology of  $\text{Ni}_{0.6}\text{Cd}_{0.4}\text{Y}_{0.075}\text{Fe}_{1.925}\text{O}_4$  by SEM

**b) TEM analysis:** The particle size was estimated using TEM analysis. The reduction in particle size with rare earth doping is evident from TEM images. Average particle sizes measured are given in table 1. Figure 4(a) and (b) show the

TEM images of  $\text{Ni}_{0.6}\text{Cd}_{0.4}\text{Y}_{0.075}\text{Fe}_{1.925}\text{O}_4$  nanoferrite by using sol-gel autocombustion method. The most of nanoparticles are in spherical shape and agglomerated due to the tendency of nano particles.

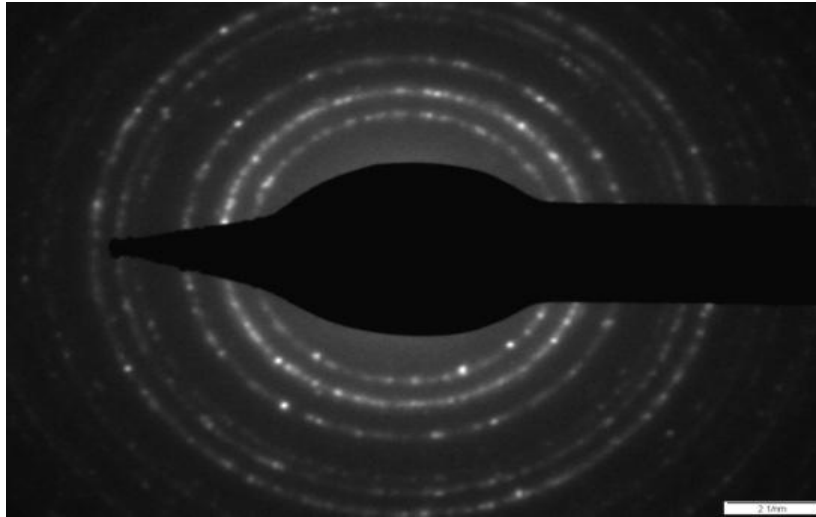


Figure 4(a): Morphology of  $\text{Ni}_{0.6}\text{Cd}_{0.4}\text{Y}_{0.075}\text{Fe}_{1.925}\text{O}_4$  by TEM

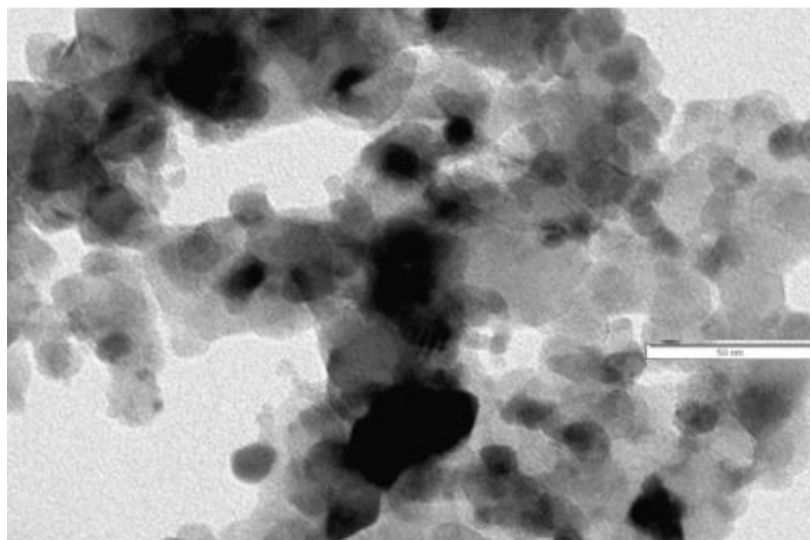


Figure 4(b): Particle size using morphology of  $\text{Ni}_{0.6}\text{Cd}_{0.4}\text{Y}_{0.075}\text{Fe}_{1.925}\text{O}_4$  by TEM

### 3.4 Electrical Studies

The DC electrical resistivity measurements on the prepared samples were carried out to get information about free and localized electric charge carriers. The conductivity was measured between the current range 1pF to 100 pF. The figure 5(a) and (b) shows that the  $\text{Y}^{3+}$  doped Ni-Cd nanoferrite impedance graph. Prepared sample shows as

current increases then the resistivity increases and conductivity decreases. For both temperature 300 °C and 200 °C figure indicates that as temperature increases the conductivity increases. Sample exhibited semiconducting nature after 600 voltage and has sudden increase in conductivity.

Table 2: The resistivity and conductivity of  $\text{Ni}_{1-x}\text{Cd}_x\text{Y}_y\text{Fe}_{2-y}\text{O}_4$

Composition	Resistivity ( $\rho$ ) (ohm-m)		Conductivity ( $\sigma$ ) (mho)	
	at 200 °C	at 300 °C	at 200 °C	at 300 °C
$\text{Ni}_{0.8}\text{Cd}_{0.2}\text{Fe}_2\text{O}_4$	301584.60	383682.00	$3.3158 \times 10^{-6}$	$2.6063 \times 10^{-6}$
$\text{Ni}_{0.8}\text{Cd}_{0.2}\text{Y}_{0.075}\text{Fe}_{1.925}\text{O}_4$	875721.76	139719.00	$1.1419 \times 10^{-6}$	$7.1572 \times 10^{-6}$
$\text{Ni}_{0.6}\text{Cd}_{0.4}\text{Y}_{0.075}\text{Fe}_{1.925}\text{O}_4$	198069.27	360828.65	$5.0487 \times 10^{-6}$	$2.7714 \times 10^{-6}$
$\text{Ni}_{0.4}\text{Cd}_{0.6}\text{Y}_{0.075}\text{Fe}_{1.925}\text{O}_4$	125902.10	153202.28	$7.9426 \times 10^{-6}$	$6.5273 \times 10^{-6}$

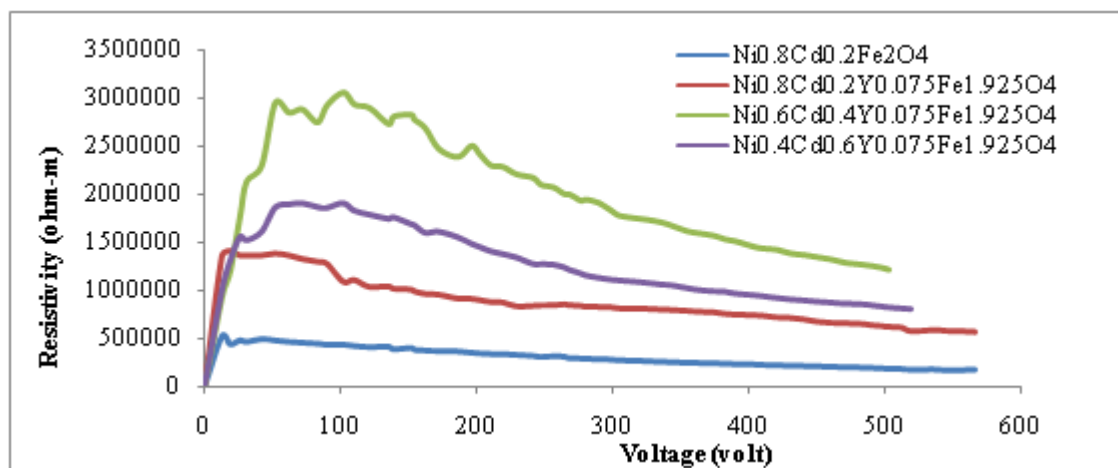


Figure 5(a): Electrical behaviour of  $\text{Ni}_{0.6}\text{Cd}_{0.4}\text{Y}_{0.075}\text{Fe}_{1.925}\text{O}_4$  at  $200\text{ }^\circ\text{C}$

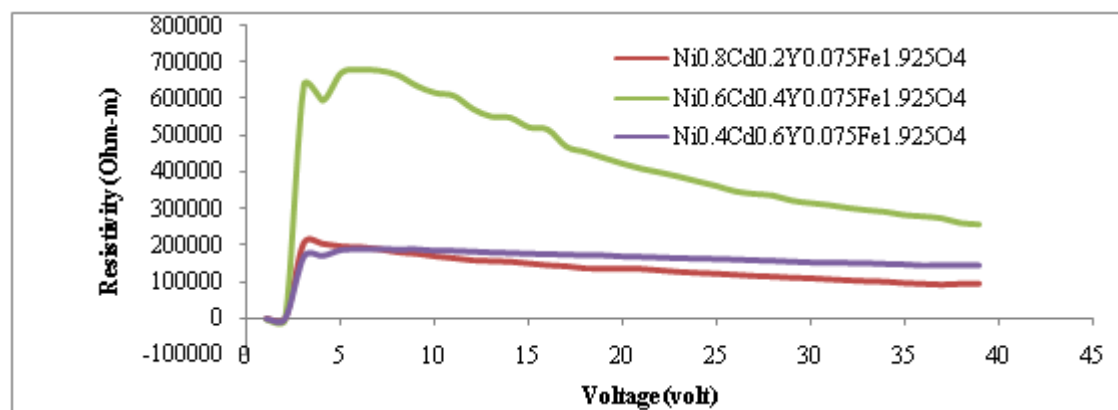


Figure 5(b): Electrical behaviour of  $\text{Ni}_{0.6}\text{Cd}_{0.4}\text{Y}_{0.075}\text{Fe}_{1.925}\text{O}_4$  at  $300\text{ }^\circ\text{C}$

Actually conductivity in ferrites are collectively contributed by electron hopping between  $\text{Fe}^{2+}$  and  $\text{Fe}^{3+}$  ions and holes hopping between  $\text{Y}^{2+}$  and  $\text{Y}^{3+}$  ions and depends on availability of charge carriers with mobility. Hence increase in conductivity explains increase in hopping pairs.

#### 4. Conclusions

Nano structured  $\text{Ni}_{1-x}\text{Cd}_x\text{Y}_y\text{Fe}_{2-y}\text{O}_4$  (where  $x=0, 0.2, 0.4, 0.6$  and  $y=0$  and  $0.075$ ) powder were successfully prepared by sol-gel autocombustion method. The structure and morphology were characterized and determined by XRD, EDAX, FTIR, SEM and TEM and confirm the formation of nano size particles. The XRD pattern shows that nanoparticles decreases with the increase in  $\text{Y}^{3+}$  content. The powders without  $\text{Y}^{3+}$  and  $\text{Cd}^{2+}$  presented small quantities of a second phase hematite ( $\text{Fe}_2\text{O}_3$ ). The optical properties of prepared sample were also investigated. The FTIR shows the characteristic bond of spinel structure. From XRD, EDAX and FTIR analysis it is confirmed that  $\text{Y}^{3+}$  doping on Ni-Cd ferrite can be prepared easily according to sol-gel procedure. The electrical properties indicate that dc conductivity increase with the increase in temperature.

#### 5. Acknowledgements

The authors are thankful to IIT, Powai (Mumbai) for providing the instrumental facilities. We are also thankful to Savitribai Phule Pune University, Abasaheb Garware, College, Pune, Modern College of Arts,

Commerce and Science College, Ganeshkhind, Pune and SRTM University, Science College, Nanded, India for providing the instrumental facilities.

#### References

- [1] Lisboa-Filho, P.N., Vila, C., Petrucelli, G., Paiva-Santos, C.O., Gama, L., Ortiz, W.A. and E. Longo (2002) *Physica B: Condensed Matter*, **320**, 249-252. DOI: 10.1016/S0921-4526(02)00676-2
- [2] Erum Pervaiz and Gul, I.H. (2013) *Journal of Physics: Conference Series*, **439**, 012015. DOI: 10.1088/1742-6596/439/1/012015
- [3] Chandan Upadhyay, Mishra, D., Verma, H., Anand, S. and Das, R.P. (2003) *Journal of Magnetism and Magnetic Materials*, **260(1)**, 188-194. [http://dx.doi.org/10.1016/S0304-8853\(02\)01320-3](http://dx.doi.org/10.1016/S0304-8853(02)01320-3)
- [4] Mozaffari, M., Amighian, J. and Darsheshdar, E., (2014) *Journal of Magnetism and Magnetic Materials*, **350**, 19-22. <http://dx.doi.org/10.1016/j.jmmm.2013.08.008>
- [5] Sattar, A.A., El-sayed, H.M., El-shokrofy, K.M. and El-tabey, (2005) *Journal of Applied Sciences*, **5**, 2005, 162-168. <http://dx.doi.org/10.3923/jas.2005.162.168>
- [6] Waldron, R.D. (1955) *Physical Review*, **99(6)**, 1727-1735. DOI: <https://doi.org/10.1103/PhysRev.99.1727>
- [7] Shirsath, S.E., Jadhav, S.S., Toksha, B.G., Patange, S.M., and Jadhav, K.M. (2011) *Scripta Materialia*,

- 64(8)**, 773-776. <http://orcid.org/0000-0002-2420-1144>
- [8] Modi, K.B., Rangolia, M.K., Chhantbar, M.C., and Joshi, H.H. (2006) *Journal of Materials Science*, **41(12)**, 7308-7318.  
<http://link.springer.com/article/10.1007/s10853-006-0929-3>
- [9] Rahimi, M., Eshraghi, M. and Kameli, P. (2014) *Ceramics International*, **40(10)**, 15569–15575.  
<http://dx.doi.org/10.1016/j.ceramint.2014.07.033>
- [10] Shobana, M.K., Nam, W. and Choe, H. (2013) *Journal of Nanoscience and Nanotechnology*, **13(5)**, 3535-3538.  
<https://www.ncbi.nlm.nih.gov/pubmed/23858896>
- [11] Jain, S.R., Adiga, K.C. and Verneker, V.P. (1981) *Combustion and Flame*, **40**, 71-79.  
[doi:10.1016/0010-2180\(81\)90111-5](https://doi.org/10.1016/0010-2180(81)90111-5)